Available online at www.sciencedirect.com

ScienceDirect

Science and Technology of MATERIALS

http://ees.elsevier.com/stmat

Science and Technology of Materials 30 (2018) 103–108

Synthesis of highly crystalline phase pure calcium metastannate by molten salt method

I.A. Disher Al-Hydary *, S.J. Edress Al-Mohana, M.M. Hussein Al-Marzooqee

Department of Ceramics and Building Materials, Collage of Materials Engineering, University of Babylon, Babylon, P.B. #4, Iraq

Received 16 February 2018; accepted 4 April 2018

Abstract

Calcium metastannate $CaSnO_3$ with orthorhombic crystal system has been synthesized at low temperature by molten salt method using KCl-LiCl as a reaction medium and equimolar of SnO_2 and $CaCO_3$ as precursors. The process parameters including the reaction temperature, salt type, and salt to precursor weight ratio were investigated. Rietveld refinements on X-ray powder diffraction patterns were performed using X'Pert HighScore Plus software to calculate phase percent of each phase present in the obtained powder. The results of these calculations were followed in order to choose the salt system that requires the least reaction temperature to produce the highest $CaSnO_3$ percent. The as-prepared compound was characterized by various techniques such as X-Ray diffraction (XRD), energy dispersive X-Ray spectrometry (EDX), Fourier transform infrared spectrometry (FTIR), and field emission scanning electron microscope (FE-SEM). The experimental results showed that highly crystalline phase pure $CaSnO_3$ laminar plates could be prepared at 1000 °C for short period of time without any other detectable secondary phases.

Keywords: Molten salt synthesis; Calcium metastannate; $CaSnO_3$; Rietveld refinement; Phase pure materials; Chloride salt system

1. Introduction

$CaSnO_3$ belongs to the family of alkaline-earth metastannates which has the chemical formula $MSnO_3$ where M is Ca, Ba or Sr. It has many outstanding properties, such as the high electrical capacity at low potentials, the photocatalytic effectiveness, the antistatic surface properties, the pollution-free and wide availability of the raw materials, and the low cost. Thus, $CaSnO_3$ has been used in many applications including the photocatalytic reforming of ethanol/water solution to hydrogen [1], the photocatalytic degradation of universal organic pollutants [2], the high capacity anode material for lithium-ion batteries [3–5], sensing element in sensors [2,6], phosphor host materials [7–9], inorganic pigments [10], energy-efficient windows, and antistatic coatings [11].

Calcium metastannate was synthesized by different methods like the solid-state reaction [4,5], the self-heat sustained reaction (SHS) [12], the sol–gel method [4], and the polymeric precursor method [13]. However, it is still difficult to prepare phase pure $CaSnO_3$ because of (i) the need for multi steps of high calcination temperature, reaches up to 1450 °C, for long period of time up to 24 hours [5,12], (ii) the use of expensive precursors and surfactants [14,15], and (iii) the formation of secondary phases such as SnO_2 and CaO [14]. In addition, some of these methods are environmentally unfriendly and cannot be scaled up to a large scale production [16].

Molten salt method has the potential to overcome these difficulties. It has been established to be straightforward, low cost, clean, and convenient method for large scale production with uniform particle morphology [17,18]. Furthermore, molten salt method has been reported for the synthesis of variety of advanced ceramic materials with different sizes and morphologies at much lowered temperatures than those reported for the other preparation methods [19–21]. Moreover, molten salt method has been used for modification [22–24] and the preparation of porous materials [25–27] and nitrides [28–31].

However, to the best of our knowledge, $CaSnO_3$ was not reported to be synthesized by molten salt method before. In the current work, phase pure $CaSnO_3$ powder is to be synthesized using molten salt method at low temperature for short period of time.

* Corresponding author.
E-mail addresses: imadali4@uobabylon.edu.iq, imadali4@yahoo.com (I.A.D. Al-Hydary).

https://doi.org/10.1016/j.stmat.2018.04.002

2. Materials and methods

All the materials and chemicals used in the current work were analytical reagents and they were used as received without farther treatment. $CaCO_3$ (Sigma–Aldrich, ≥99% purity), SnO_2 (Sigma-Aldrich, 99.9% purity) were used for preparing $CaSnO_3$ powder. In the first step, equimolar amounts of SnO_2 and $CaCO_3$ were mixed with the desired salt system for five minutes using agate mortar with salt to precursor weight ratio (S:P) of (1:1), (3:1), and (5:1). Then, the mixture was transferred into alumina crucible with alumina lid and heat treated at temperatures of 850 °C and 1000 °C for 3 h. The product was washed thoroughly with hot distilled water for 5 times in order to remove any residual chloride salts.

Six types of salt systems were used including (NaCl, KCl, LiCl, NaCl-KCl, NaCl-LiCl, KCl-LiCl). To select the appropriate salt system, the criterion was the need for the minimum synthesis temperature to produce the highest percent of $CaSnO_3$. Rietveld refinement calculations were used to calculate the percent of each phase present in the resulting powders. After choosing the appropriate salt system, many experiments were carried out to find out the appropriate reaction temperature.

Phase identification and the calculations of the amount of each phase present were carried out using XRD analysis and Rietveld refinement. The patterns were recorded at room temperature using (Shimadzu 6000 diffractometer) equipped with Cu-Kα radiation (λ = 0.15406 nm) operated at 40 kV and 30 mA. Rietveld refinements on X-Ray powder diffraction patterns were performed using X'Pert HighScore Plus software. Powder morphology including the size and shape of the prepared particles was observed by field emission scanning electron microscopy (FE-SEM) with a MIRA3 instrument. The purity of the obtained compound was confirmed using energy dispersive X-ray spectrometry (EDS) using TESCAN instrument. Fourier transformed infrared spectra (FTIR) of the samples were recorded using (Shimadzu 1800, Japan) to evaluate molecular structure of the functional group in prepared powder. The specific surface area measurements by Nitrogen adsorption/desorption isotherms were obtained with an (QSURF surface area analyzer) apparatus.

3. Results and discussion

3.1. Selecting the salt system

In the initial stage of the experiments and in order to identify the best salt system to be used in the preparation of $CaSnO_3$, six patches of chlorides salt were tested including (NaCl, KCl, LiCl, NaCl-KCl, NaCl-LiCl, KCl-LiCl). Fig. 1 shows the XRD patterns of samples prepared with (3:1) S:P ratio at 850 °C for 3 h, using different salt systems. LiCl was disqualified due to the very low intensity of $CaSnO_3$. The KCl, NaCl and NaCl-KCl were excluded due to high intensity of SnO_2. (NaCl-LiCl) and (KCl-LiCl) salt systems gave results close to each other, therefore Rietveld refinement for quantitative analysis were used to choose the best salt system according to the amount of $CaSnO_3$ obtained for each salt system at the same conditions.

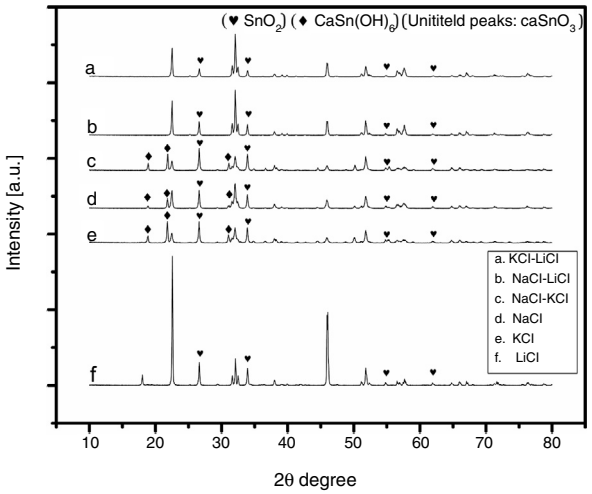

Fig. 1. XRD patterns of $CaSnO_3$ prepared in different salt systems.

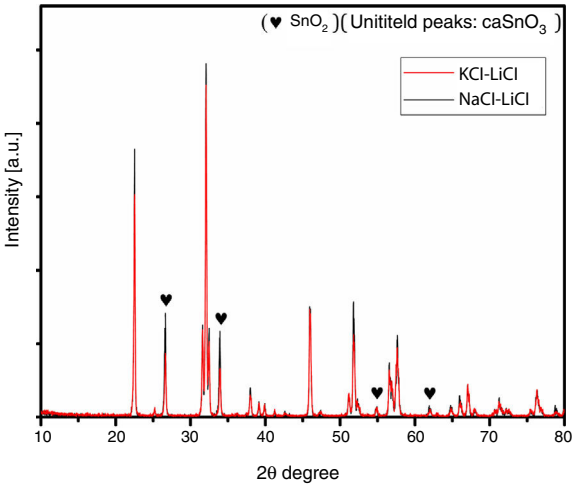

Fig. 2. XRD comparison between (NaCl-LiCl and KCl-LiCl).

Fig. 2 shows a comparison between the XRD patterns of the samples prepared in (NaCl-LiCl) and (KCl-LiCl) salt systems. All peaks are corresponding to $CaSnO_3$ (ICSD card 98-008-9855) and SnO_2 (ICSD card 98-005-7566). The (NaCl-LiCl) salt system gives better crystallinity as compared with (KCl-LiCl), but the intensity of SnO_2 was also high. In order to select the more appropriate salt system, the relative intensity ratio (RIR) was considered. The highest intensity of $CaSnO_3$ at (32.066°) was divided by the highest intensity of SnO_2 at (26.611°) to obtain the RIR; the highest RIR ratio means better $CaSnO_3$ formation and subsequently better salt system. It has been found that the RIR in the case of (KCl-LiCl) is (1063.87/203.65 = 5.224) while that in the case of (NaCl-LiCl) is (1168.78/339.87 = 3.439). Based on that, (KCl-LiCl) salt system was selected as the more appropriate salt system. These results were confirmed using Rietveld refinement for quantitative analysis as shown in (Table 1).

Table 1
Rietveld refinement data obtained after XRD analyses for powders calcined at 850 °C for 3 h.

Salt system	Phase amount (wt.%)		
	$CaSnO_3$	SnO_2	$CaSn(OH)_6$
NaCl-LiCl	82.6	17.4	0
KCl-LiCl	87.7	12.3	0
NaCl-KCl	45.5	37.1	17.4
LiCl	70.1	29.9	0
KCl	47.3	32.3	20.4
NaCl	66	26.2	7.8

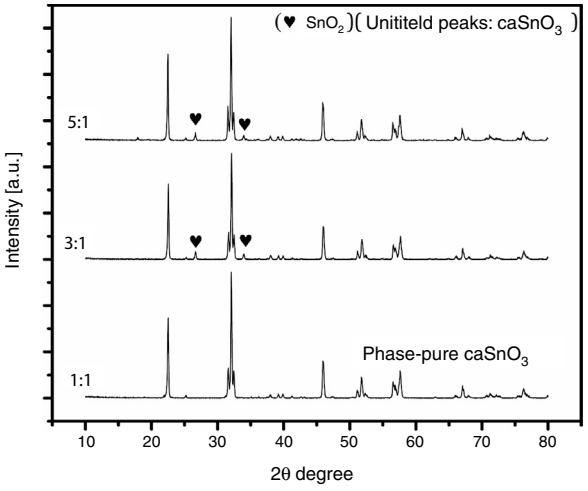

Fig. 3. XRD patterns of $CaSnO_3$ samples prepared with different S:P ratios in (KCl-LiCl) salt system at 1000 °C for 3 h.

3.2. Effect of S:P ratio

To study the effect of salt content on the resulting powder, three different ratios were used; these are (1:1, 3:1 and 5:1). Fig. 3 shows the XRD patterns for samples prepared with different S:P ratios in (KCl-LiCl) salt system at 1000 °C for 3 h. When the S:P ratio of 1:1 is used, the XRD peaks are indexed to phase pure perovskite orthorhombic CaSnO3 (ICSD card 98-008-9855). This implies that the presence of molten (KCl–LiCl) with S:P ratio of (1:1) salt system can indeed accelerate the kinetics and facilitate the formation of $CaSnO_3$ at 1000 °C. While, increase the S:P ratio from (1:1) to (3:1) or (5:1) enhances the formation of SnO_2, this could be attributed to the reduction of Sn by the chlorine which is formed upon decomposition of the salt and the evaporation of the chlorine. At high temperatures, chlorine can be eliminated from the salt according to Eq. (1). This can lead to the reduction of tin in accordance with Eq. (2). Due to this process, tin oxide (SnO) can be produced as a secondary phase [13] which, in turn, converted to SnO_2 due to the thermal treatment at high temperatures in O_2 atmosphere as reported by many researchers [32–34].

$$2Cl^- \rightarrow Cl_2(g) + 2e^- \quad (1)$$

$$Sn^{4+} + 2e^- \rightarrow Sn^{2+} \quad (2)$$

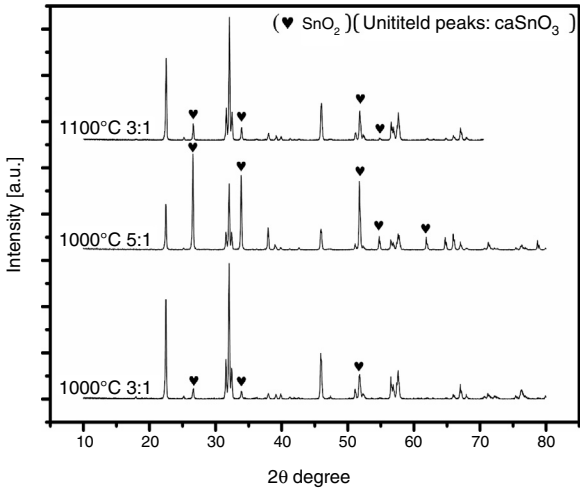

Fig. 4. XRD pattern of $CaSnO_3$ samples prepared with different S:P ratios and different reaction temperatures in (NaCl-LiCl) salt system.

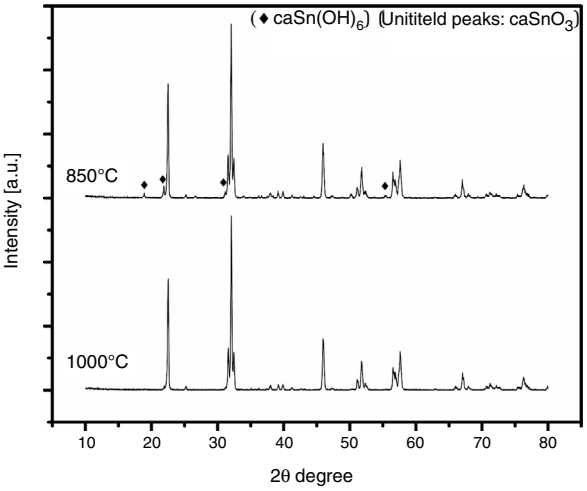

Fig. 5. XRD pattern of $CaSnO_3$ samples prepared with S:P ratio of 1:1 at 850 °C and 1000 °C.

To ensure this explanation and to remove any ambiguity next trail was done with the second salt system (NaCl-LiCl). In this trail, high S:P ratios of (3:1) and (5:1) at temperature of 1000 °C for 3 h were used, also, S:P ratio of (3:1) at higher temperature of 1100 °C for 3 h was tested. It is well-known that with increase the salt content or calcination temperature, the evaporation of chloride increases. The choice of the second best chloride salt was to make sure of the concept that Sn reduction happens with any chloride salt system as shown in Fig. 4.

Analysis of Fig. 4 shows that with increase the salt content from (3:1) to (5:1), SnO_2 content increases. Also upon increase reaction temperature from 1000 °C to 1100 °C, SnO_2 content also increases. It was also noticed that the salt content (S:P) is more effective than reaction temperature. These results confirm the earlier explanation of Sn reduction.

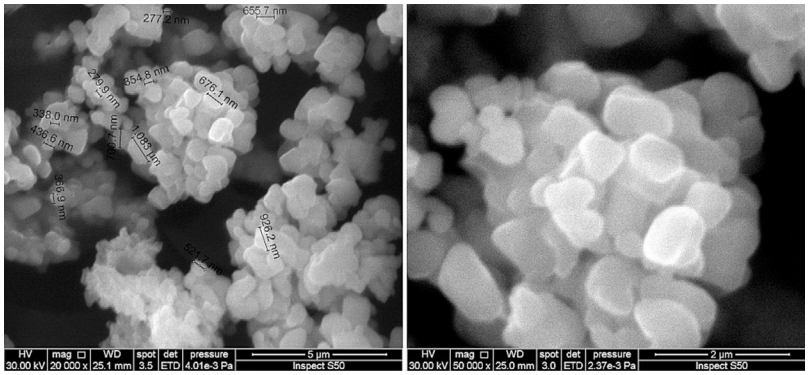

Fig. 6. SEM images of the phase impure $CaSnO_3$ obtained at 850 °C in (KCl-LiCl) salt system with S:P of (1:1).

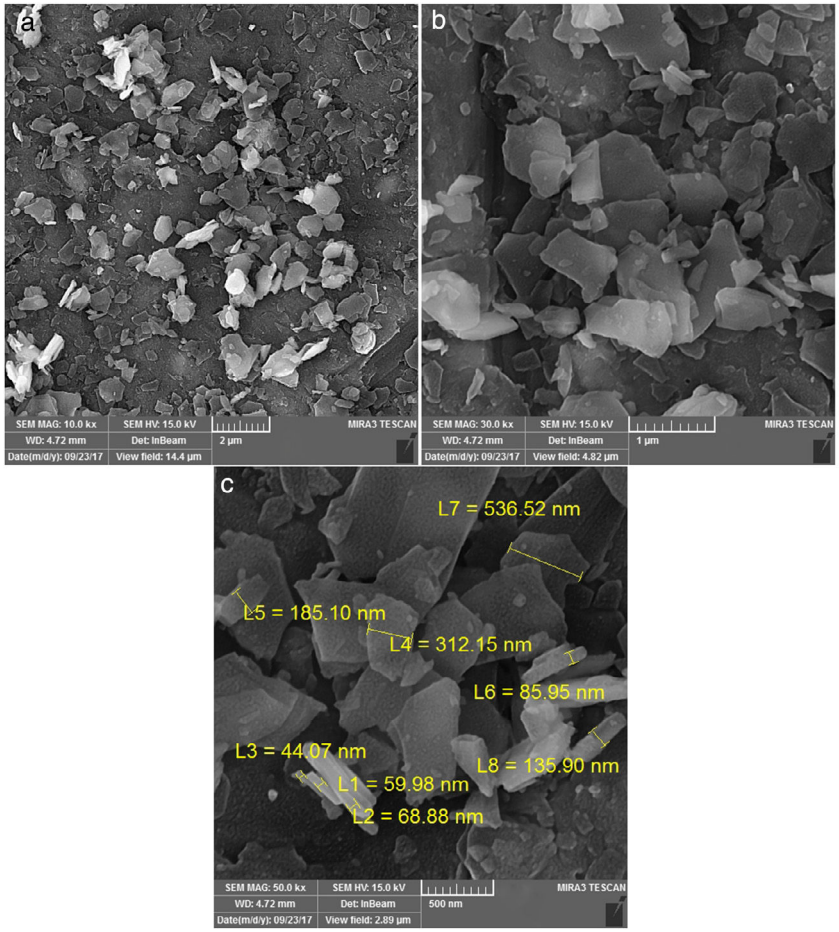

Fig. 7. FE-SEM images of phase pure $CaSnO_3$ sample prepared with S:P of (1:1) at 1000 °C for 3 h.

3.3. *Effect of reaction temperature*

Fig. 5 shows the XRD patterns of $CaSnO_3$ samples prepared with S:P ratio of (1:1) at different reaction temperatures of 850 °C and 1000 °C. XRD results and Rietveld refinement shows that the resulting powder prepared at 850 °C is comprised of two phases: (97.7%) $CaSnO_3$ with (2.3%) of Burtite ($CaSn(OH)_6$, ICSD card no. 98-001-2665), while phase pure perovskite orthorhombic $CaSnO_3$ is obtained at 1000 °C.

SEM results of phase impure $CaSnO_3$ obtained at 850 °C in (KCl-LiCl) salt system with S:P ratio of (1:1) is shown in Fig. 6. The agglomerates consist of polyhedral particles with some faceting, which suggests limited crystallinity, and have an average particle size less than 1 μm.

Fig. 7 from A-C shows the FE-SEM images at different magnifications to the phase pure $CaSnO_3$ obtained at 1000 °C in (KCl-LiCl) salt system with S:P ratio of (1:1). The resulting powder is composed of laminar plates with low aspect ratio.

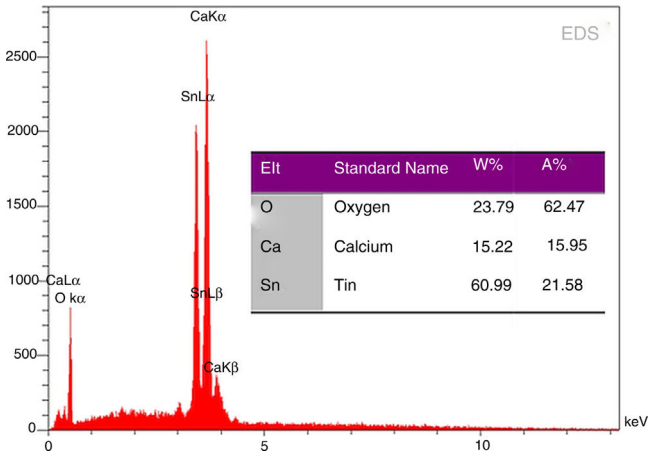

Fig. 8. EDS analysis of phase pure $CaSnO_3$ prepared with S:P ratio of (1:1) at 1000 °C for 3 h.

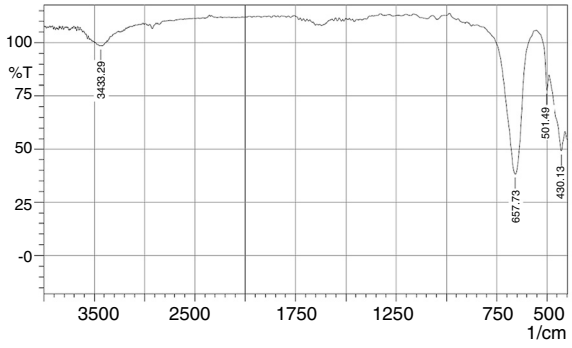

Fig. 9. FTIR spectra of phase pure $CaSnO_3$ prepared with S:P ratio of (1:1) at 1000 °C for 3 h.

By comparing the SEM images from Fig. 6 with that in Fig. 7 different morphologies can be observed. This shows the effect of temperature on the powder morphology. This effect points out a promising way to synthesize different morphologies and sizes of $CaSnO_3$ in the molten (KCl–LiCl) salt system.

EDS analysis of phase pure $CaSnO_3$ prepared at 1000 °C in (KCl-LiCl) salt system with S:P ratio (1:1) is shown in Fig. 8. The EDS results show clearly the prepared $CaSnO_3$ is chemically pure without any detectable impurities which involved in other preparation methods as the presence of carbonates [35] or the contaminations coming from milling process as in the work of Mary C.F. Alves et al. (2007) where they obtained powder contains high quantity of carbon when synthesis $CaSnO_3$ powder by polymeric precursor method; therefore, powder needs farther heat treatment at 250 °C for 12 h in oxygen atmosphere to eliminate carbon from the produced powder.

The BET surface area of the phase pure $CaSnO_3$ is (0.62 m^2/g) reflecting the large particle size of the prepared powder.

The FT-IR spectra of the phase pure $CaSnO_3$ is depicted in Fig. 9. The peak at 3433 cm^{-1} is responsible for hydroxyl adsorbed on the surface of particles which could be due to moisture absorption during testing (physisorbed) [15,36]. The appearance of strong IR absorption band at 430 cm^{-1} is attributed to the lattice vibrations of Ca-O [37]. Absorption band at 501 cm^{-1} and 657 cm^{-1} is attributed to symmetric vibrations of SnO_6 octahedra [38] and stretching vibrations of Sn–O–Sn [39], respectively. In addition, the IR band at around 3568 cm^{-1} for the stretching mode of $Sn(OH)_2$ is not detected as confirmed by XRD test for the synthesized phase pure Calcium metastannate powder [38].

4. Conclusions

Highly crystalline phase pure calcium metastannate can be synthesized by molten salt method at 1000 °C for 3 h. SnO_2 and $CaCO_3$ are suitable precursors in (KCl-LiCl) salt system with S:P ratio of (1:1). It was found that the salt content has a great effect on the synthesis process especially on the reduction of SnO_2 due to chlorination effect. The firing condition is 200 °C less than solid state reaction method and with much shorter time.

Acknowledgement

The authors gratefully acknowledge the College of Materials Engineering, University of Babylon for support and encouragement to carry out this study.

References

[1] F. Zhong, et al., Structural evolution of alkaline earth metal stannates $MSnO_3$ (M = Ca, Sr, and Ba) photocatalysts for hydrogen production, RSC Adv. 6 (48) (2016) 42474–42481.
[2] W. Wang, et al., Hydrothermal synthesis and catalytic performances of a new photocatalyst $CaSnO_3$ with microcube morphology, Scr. Mater. 60 (3) (2009) 186–189.
[3] S. Zhao, Y. Bai, W.-F. Zhang, Electrochemical performance of flower-like $CaSnO_3$ as high capacity anode material for lithium-ion batteries, Electrochim. Acta 55 (12) (2010) 3891–3896.
[4] N. Sharma, et al., Sol–gel derived nano-crystalline $CaSnO_3$ as high capacity anode material for Li-ion batteries, Electrochem. Commun. 4 (12) (2002) 947–952.
[5] M. Mouyane, et al., Original electrochemical mechanisms of $CaSnO_3$ and $CaSnSiO_5$ as anode materials for Li-ion batteries, J. Solid State Chem. 184 (11) (2011) 2877–2886.

[6] P.T. Moseley, et al., Electrical conductivity and gas sensitivity of some transition metal tantalates, Sens. Actuators 14 (1) (1988) 79–91.
[7] G. Katsuhiko, Y. Nakachi, K. Ueda, Photoluminescence properties of Pr doped and Tb–Mg codoped $CaSnO_3$ with perovskite structure, Thin Solid Films 516 (17) (2008) 5885–5889.
[8] Z. Liu, Y. Liu, Synthesis and luminescent properties of a new green afterglow phosphor $CaSnO_3$:Tb, Mater. Chem. Phys. 93 (1) (2005) 129–132.
[9] A. Stanulis, et al., Photoluminescence of Pr^{3+}-doped calcium and strontium stannates, J. Luminesc. 172 (2016) 323–330.
[10] Ž. Dohnalová, P. Šulcová, M. Trojan, Preparation and selected properties of pigments on base of Ln-doped $CaSnO_3$, J. Therm. Anal. Calorim. 93 (3) (2008) 857–861.
[11] H. Mizoguchi, P.M. Woodward, Electronic structure studies of main group oxides possessing edge-sharing octahedra: implications for the design of transparent conducting oxides, Chem. Mater. 16 (25) (2004) 5233–5248.
[12] L.L. Shyan, M.A. Alim, Immittance response of $CaSnO_3$ prepared by self-heat-sustained reaction, J. Mater. Sci. 34 (6) (1999) 1175–1187.
[13] M. Alves, et al., Influence of the precursor salts in the synthesis of $CaSnO_3$ by the polymeric precursor method, J. Therm. Anal. Calorim. 87 (3) (2007) 763–766.
[14] V. Berbenni, et al., Synthesis of calcium metastannate ($CaSnO_3$) by solid state reactions in mechanically activated mixtures calcium citrate tetra hydrate [$Ca_3(C_6H_5O_7)_2{\cdot}4H_2O$]–tin (II) oxalate ($SnC_2O_4$), Thermochim. Acta 608 (2015) 59–64.
[15] S. Moshtaghi, M. Salavati-Niasari, D. Ghanbari, Characterization of $CaSn(OH)_6$ and $CaSnO_3$ nanostructures synthesized by a new precursor, J. Nanostruct. 5 (2) (2015) 169–174.
[16] A. Stanulis, et al., Sol–gel (combustion) synthesis and characterization of different alkaline earth metal (Ca, Sr, Ba) stannates, J. Sol-Gel Sci. Technol. 64 (3) (2012) 643–652.
[17] M. Khangkhamano, c and ZrC Powders and Molten Salt Synthesis of Novel TiC (PhD diss.), University of Exeter, 2014.
[18] C. Sheikh, The Synthesis of Cementitious Compounds in Molten Salts (PhD diss.), UCL (University College London), 2016.
[19] W. Qiu, et al., Molten salt synthesis and growth mechanism of WC platelet powders, Powder Technology 310 (2017) 228–233.
[20] R. Fazli, F. Golestani-Fard, The effects of processing parameters on molten salt synthesis of $CaZrO_3$ nano-powders using oxide precursors, Powder Technol. 257 (2014) 149–155.
[21] B. Roy, P.A. Fuierer, S. Aich, Synthesis of TiO_2 scaffold by a 2 step bi-layer process using a molten salt synthesis technique, Powder Technol. 208 (3) (2011) 657–662.
[22] J. Ding, D. Guo, C.J. Deng, H.X. Zhu, C. Yu, Low-temperature synthesis of nanocrystalline ZrC coatings on flake graphite by molten salts, Appl. Surf. Sci. 407 (2017) 315–321.
[23] J. Ding, C.J. Deng, W.J. Yuan, H.X. Zhu, X.J. Zhang, Novel synthesis and characterization of silicon carbide nanowires on graphite flakes, Ceram. Int. 40 (2014) 4001–4007.
[24] J. Ding, C.J. Deng, W.J. Yuan, H.X. Zhu, J. Li, The synthesis of titanium nitride whiskers on the surface of graphite by molten salt media, Ceram. Int. 39 (2013) 2995–3000.
[25] X.Q. Kan, J. Ding, C. Yu, H.X. Zhu, C.J. Deng, G.Y. Li, Low-temperature fabrication of porous ZrC/C composite material from molten salts, Ceram. Int. 43 (2017) 6377–6384.
[26] J. Ding, H.X. Zhu, C.J. Deng, G.Q. Li, K.L. Wang, J.P. Liu, Preparation and characterisation of porous biomorphic SiC/C ceramic from molten salt, Ceram. Int. 41 (2015) 11539–11545.
[27] J. Ding, H.X. Zhu, G.Q. Li, C.J. Deng, J. Li, Growth of SiC nanowires on wooden template surface using molten salt media, Appl. Surf. Sci. 320 (2014) 620–626.
[28] X.Q. Kan, J. Ding, H.X. Zhu, C.J. Deng, Y. Chao, Low temperature synthesis of nanoscale titanium nitride via molten-salt-mediated magnesiothermic reduction, Powder Technol. 315 (2017) 81–86.
[29] J.P. Liu, J. Ding, H.X. Zhu, C.J. Deng, Z.N. Chai, Effect of NH_4Cl addition on the morphology of beta-SiAlON powders prepared by salt-assisted nitridation, J. Ceram. Soc. Jpn. 125 (3) (2017) 155–158.
[30] J. Ding, H.X. Zhu, G.Q. Li, C.J. Deng, Z.N. Chai, Catalyst-assisted synthesis of alpha-Si_3N_4 in molten salt, Ceram. Int. 42 (2016) 2892–2898.
[31] Z.N. Chai, J. Ding, C.J. Deng, H.X. Zhu, G.Q. Li, Y. Chao, Ni-catalyzed synthesis of hexagonal plate-like alpha silicon nitride from nitridation of Si powder in molten salt media, Adv. Powder Technol. 27 (2016) 1637–1644.
[32] C.S. Lim, A solvothermal process to synthesize barium metastannate nanoparticles assisted by microwave irradiation, Asian J. Chem. 25 (5) (2013) 2363.
[33] J. Geurts, S. Rau, W. Richter, F.J. Schmitte, SnO films and their oxidation to SnO_2: Raman scattering, IR reflectivity and X-ray diffraction studies, Thin Solid Films 121 (3) (1984) 217–225.
[34] M.H.M. Reddy, S.R. Jawalekar, A.N. Chandorkar, The effect of heat treatment on the structural properties of electron-beam-evaporated SnO_2 films, Thin Solid Films 169 (1) (1989) 117–126.
[35] W. Choi, H. Sung, K. Kim, J. Cho, Oxidation process from SnO to SnO_2, J. Mater. Sci. Lett. 16 (19) (1997) 1551–1554.
[36] S. Shojaei, S.A. Hassanzadeh-Tabrizi, M. Ghashang, Reverse microemulsion synthesis and characterization of $CaSnO_3$ nanoparticles, Ceram. Int. 40 (7) (2014) 9609–9613.
[37] M.I. Zaki, et al., Influence of phosphonation and phosphation on surface acid–base and morphological properties of CaO as investigated by in situ FTIR spectroscopy and electron microscopy, J. Colloid Interface Sci. 303 (1) (2006) 9–17.
[38] W. Xie, L. Zhao, Production of biodiesel by transesterification of soybean oil using calcium supported tin oxides as heterogeneous catalysts, Energy Convers. Manag. 76 (2013) 55–62.
[39] L. Wang, et al., In situ preparation of SnO2@ polyaniline nanocomposites and their synergetic structure for high-performance supercapacitors, J. Mater. Chem. A 2 (22) (2014) 8334–8341.